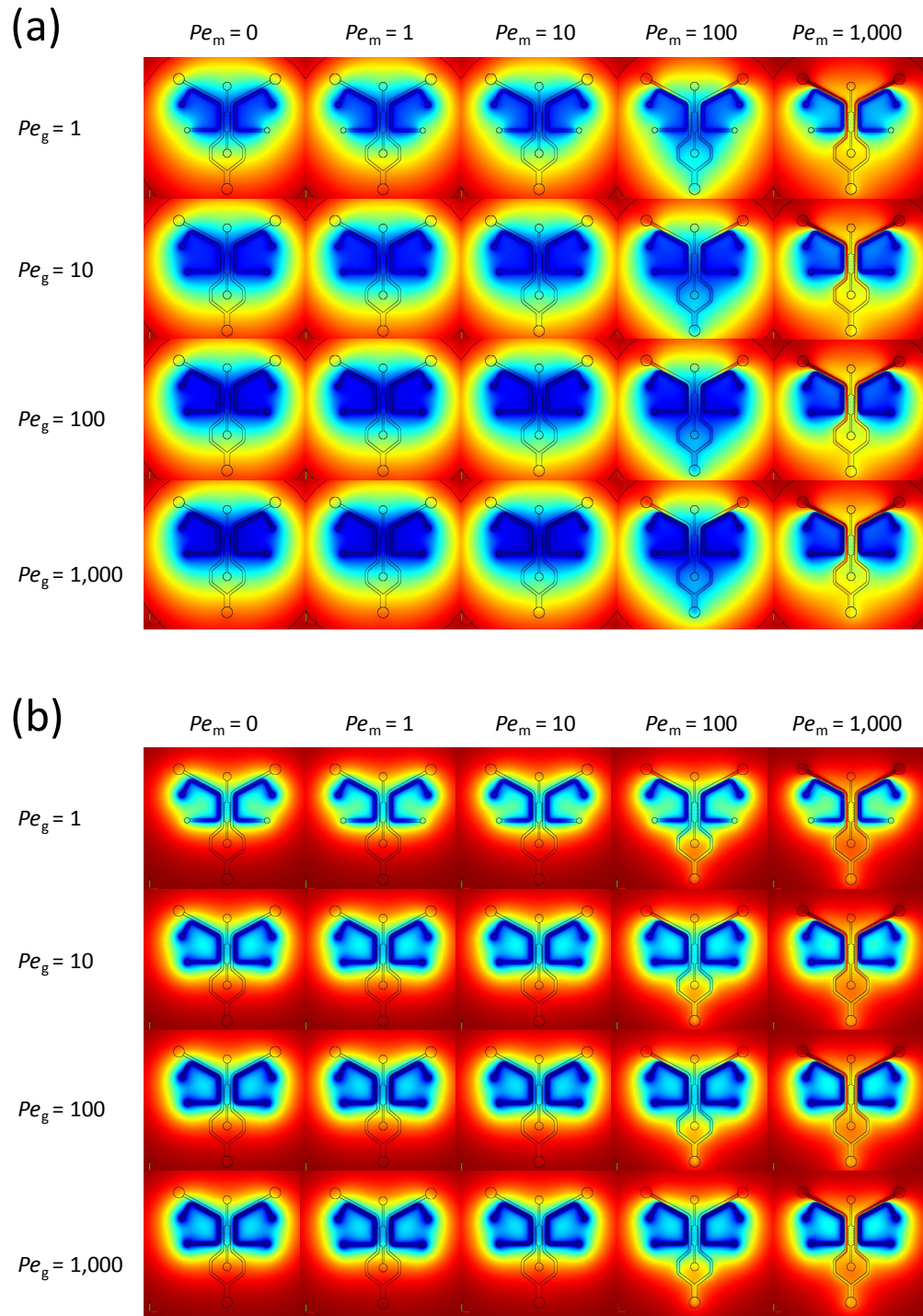
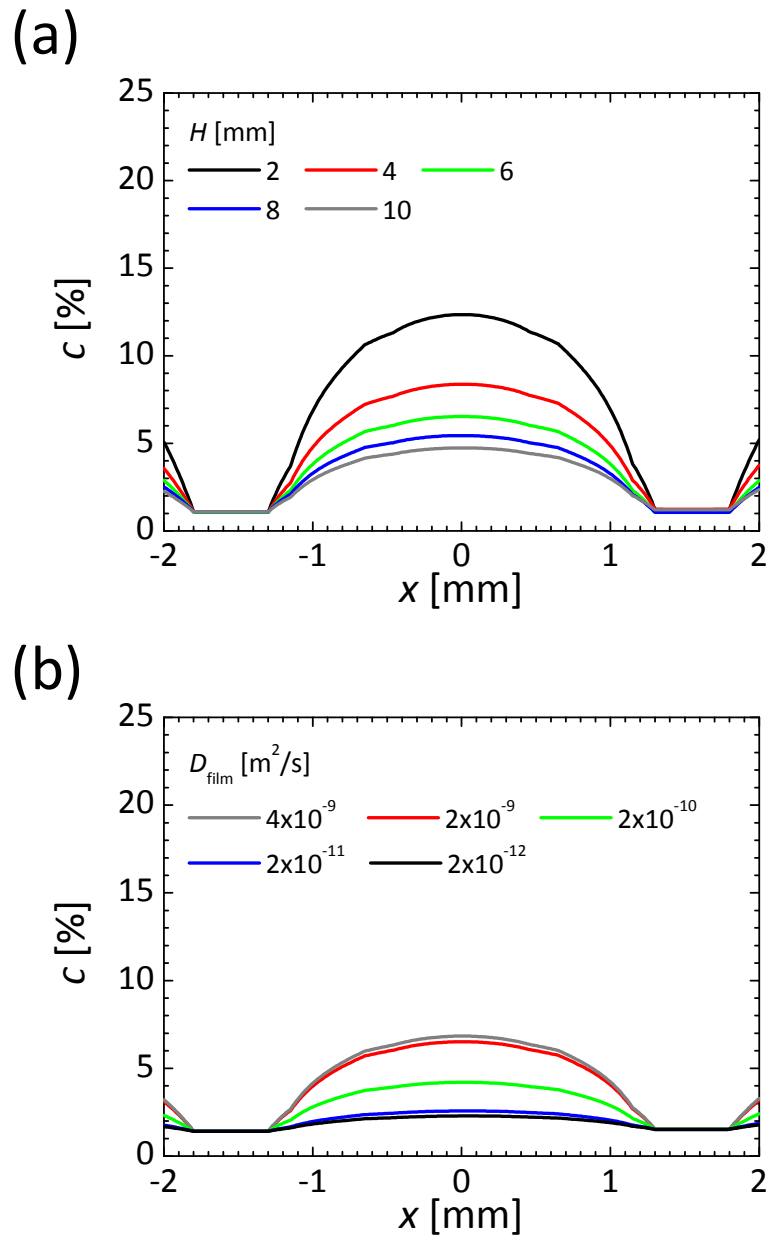


**Figure S1.** Contour map of oxygen tension at the center of the gel region on a glass cover slip,  $(x, y, z) = (0 \text{ m}, 1.975 \times 10^{-3} \text{ m}, 1 \times 10^{-6} \text{ m})$ , in the microfluidic device without a film with a combination of Péclet numbers for media and gas flow, supplying 0% oxygen gas to both gas channels.



**Figure S2.** Variations of steady oxygen tension on a crosssection ( $z = 1.0 \times 10^{-6}$  m) of the microfluidic devices (a) with and (b) without a film of low diffusion coefficient of oxygen ( $D_{\text{film}} = 2.0 \times 10^{-12}$  m<sup>2</sup>/s) with a combination of Péclet numbers for media and gas flow, supplying 0% oxygen gas to both gas channels.



**Figure S3.** Variations of oxygen tension profile across the middle of the gel region,  $(y, z) = (1.975 \times 10^{-3} \text{ m}, 1 \times 10^{-6} \text{ m})$ , in the microfluidic device at media and gas flow rates of  $(Pe_m, Pe_g) = (10, 100)$  with parameters: (a) the device of different thickness without a film, and (b) the device with a film of different diffusion coefficient of oxygen ( $H = 6$  mm).

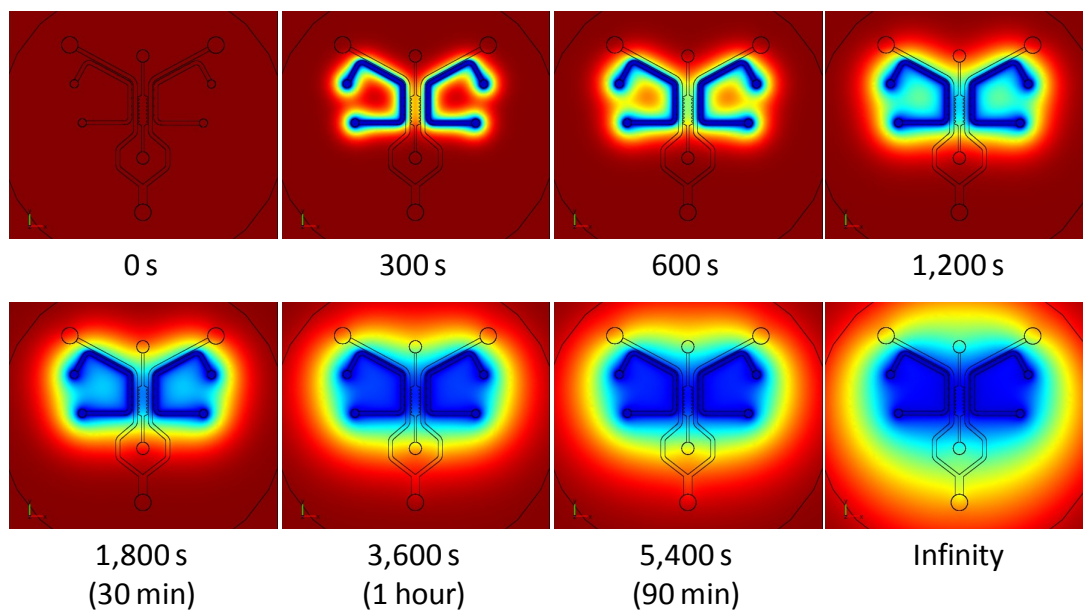


**Figure S4.** Transient change of oxygen tension on a crosssection ( $z = 1.0 \times 10^{-6}$  m) of the microfluidic device with a film of low diffusion coefficient ( $D_{\text{film}} = 2.0 \times 10^{-12}$  m<sup>2</sup>/s), supplying 0% oxygen gas to both gas channels.

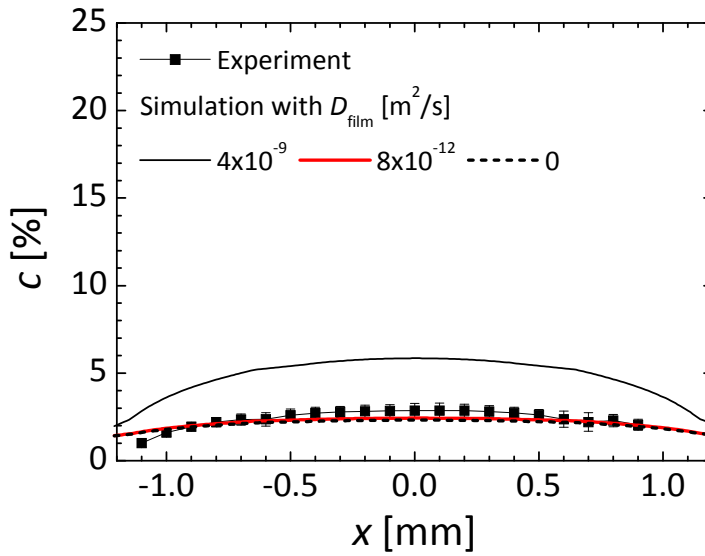


**Figure S5.** Comparison of steady oxygen tension profiles across the gel region between the experiment and the corresponding numerical simulations with three different diffusion coefficients of oxygen in a film, supplying 0% oxygen gas to both gas channels. The three different values of  $D_{\text{film}} = 4.0 \times 10^{-9} \text{ m}^2/\text{s}$ ,  $8.0 \times 10^{-12} \text{ m}^2/\text{s}$ , and  $0 \text{ m}^2/\text{s}$  correspond to the microfluidic device with no film, with a PC film having the literature value of the diffusivity, or with a film having no diffusivity of oxygen, respectively.

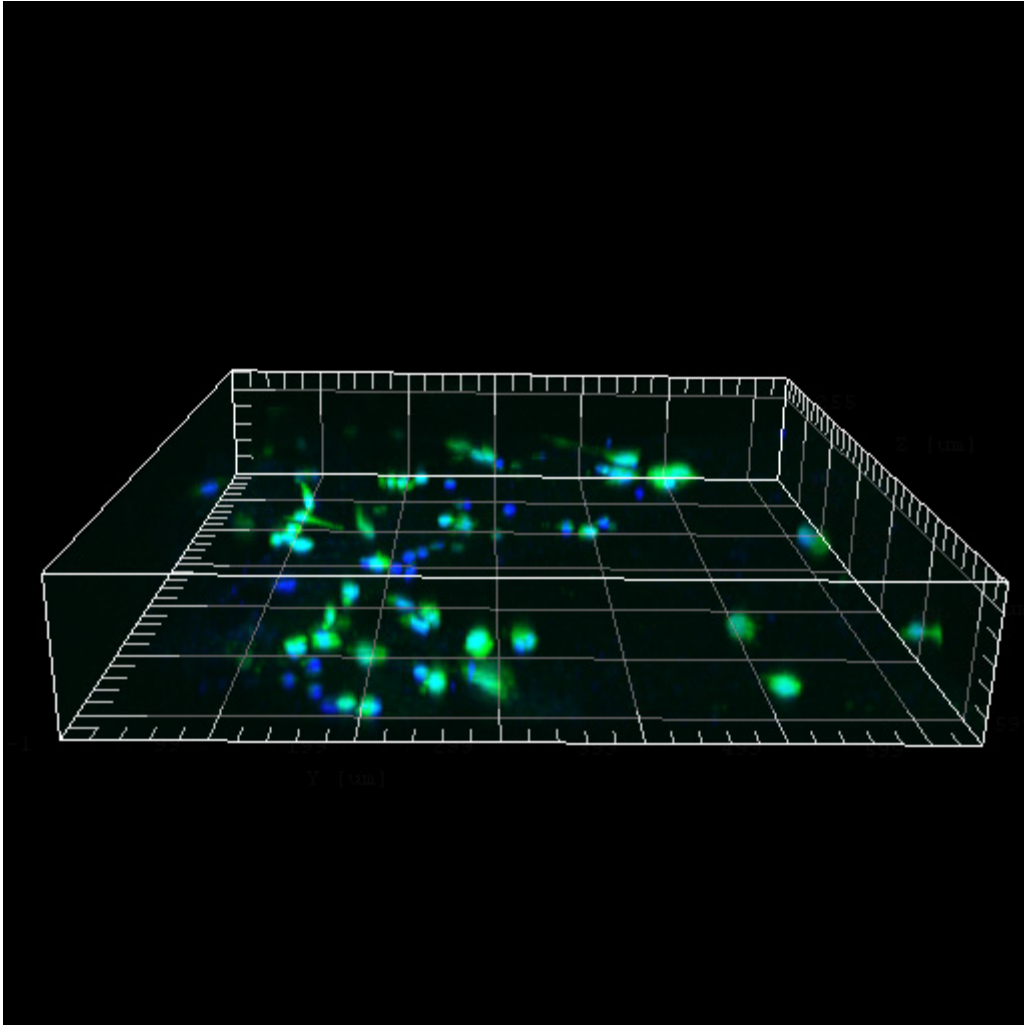


**Figure S6.** 3D confocal rendering of tumor cell distribution in the device. Tumor cells express GFP (green) and are stained for nucleus (blue: DAPI).

(2-5')

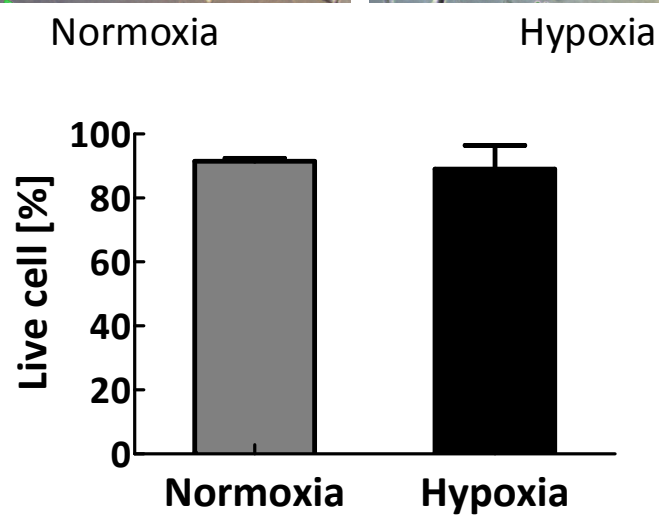
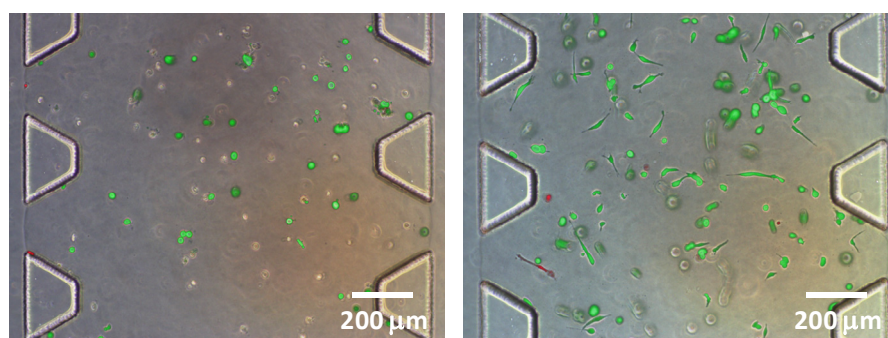


**Figure S7.** Live/dead assay of the cancer cells in the microfluidic device after 24-hr normoxia/hypoxia. Average values of four devices in each condition, and error-bars represent SEM.

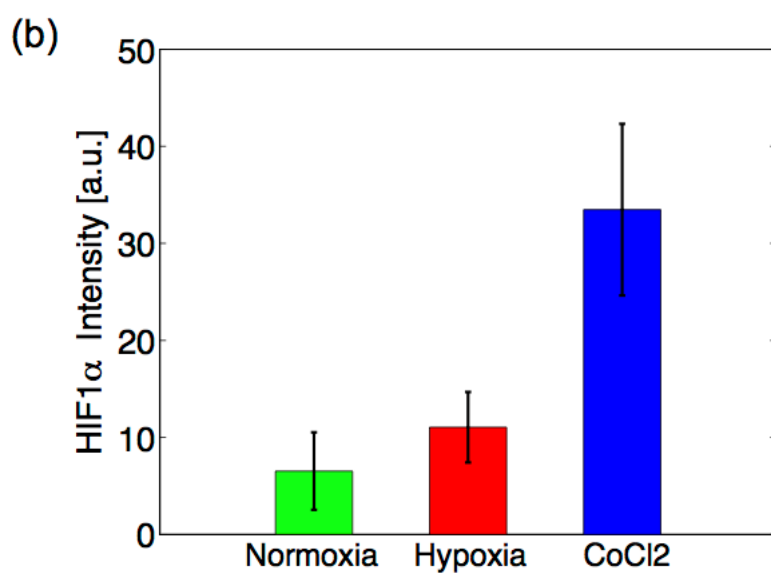
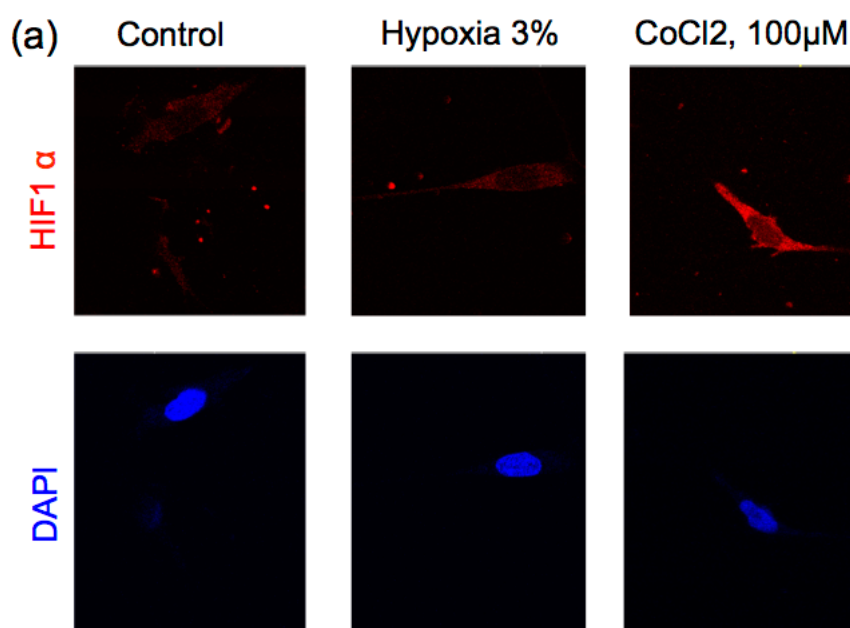
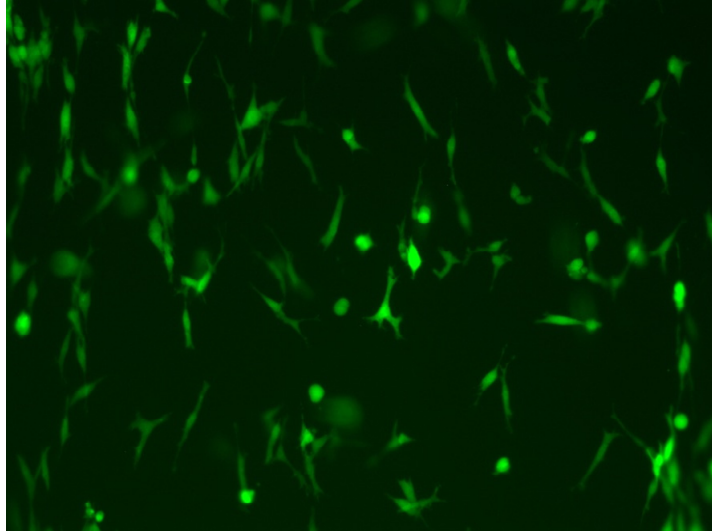


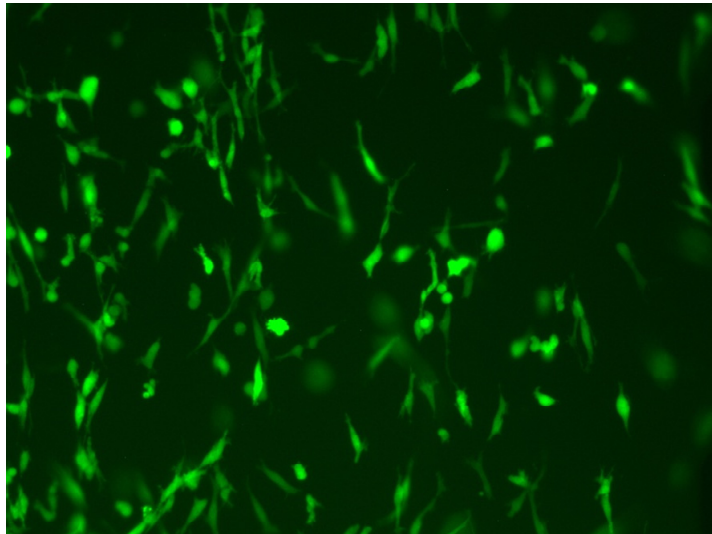
**Figure S8.** Characterization of HIF-1 $\alpha$  in the microfluidic device: (a) Top row: Staining against HIF-1 $\alpha$  under control (normoxia), hypoxia and stimulation with CoCl<sub>2</sub>; Bottom row: DAPI staining to indicate nucleus localization. (b) Quantification of images in (a), error-bars represent standard deviation.



(a)



(b)



**Movie S1.** The time-lapse images of migration of the MDA-MB-231 breast cancer cells for six hrs under (a) normoxia and (b) hypoxia.